Aerodynamic Load Alleviation Using Mini-tabs

D. J. Heathcote[1], I. Gursul[2], D. J. Cleaver[3]

Department of Mechanical Engineering, University of Bath, BA2 7AY, UK

Increased aerodynamic loads during gusts, turbulence and maneuvers define the outer envelope of aircraft structural design. Mini-tabs, small spanwise strips that protrude normal to the airfoil's upper surface, have been studied to alleviate this requirement. To investigate the mini-tab's steady state effects, force and Particle Image Velocimetry measurements were conducted at Re = 6.6 x 10^5 on a NACA0012 airfoil. Mini-tabs of height, h/c = 0.02 and 0.04 were placed at a wide range of chordwise locations. In general, the optimum location for peak lift reduction moves towards the leading edge as the angle of attack increases, with significant effect on the lift curve gradient. Trailing edge placement was effective at small angles. Placement close to the mid-chord provided a constant effect across $0° \leq \alpha \leq 5°$. For both locations, the baseline flow separation progresses ahead of the mini-tab with increasing α, which reduced effectiveness at stall. In comparison, placement close to the leading edge, x_f/c = 0.08, was ineffective for small α. At high α, a large flow separation reduced lift by up to $\Delta c_l \approx$ -0.67, but increased the unsteady forces.

[1] Postgraduate Student, Department of Mechanical Engineering. Student Member AIAA.
[2] Professor, Department of Mechanical Engineering. Associate Fellow AIAA.
[3] Lecturer, Department of Mechanical Engineering. Member AIAA.

Nomenclature

α	=	angle of attack
b	=	span
c	=	airfoil chord length
c_l	=	time-averaged lift coefficient
$c_{l\alpha}$	=	lift curve gradient, $dc_l/d\alpha$
f	=	actuation or gust frequency
h	=	mini-tab height
k	=	reduced frequency, $\pi fc/U_\infty$
n	=	exponent for the theoretical relationship
U_∞	=	free-stream velocity
ρ	=	fluid density
q	=	parameter for the theoretical relationship
Re	=	Reynolds number, $\rho U_\infty c/\mu$
u	=	velocity component parallel to free-stream
v	=	velocity component perpendicular to free-stream
μ	=	dynamic viscosity
x	=	chordwise location
x_f	=	mini-tab chordwise location
y	=	position perpendicular to free-stream
z	=	spanwise location

1. Introduction

Increased aerodynamic loads due to gusts, turbulence and maneuvers are one of the defining factors in aircraft structural design. These loads necessitate an increased structural capacity and thus mass. The field of aerodynamic load control aims to alleviate the loads at the first point of contact, reducing those passed to the structure. This could allow for a relaxation in the structural requirements, reducing airframe mass. It has been suggested [1] that application of gust and maneuver load alleviation technologies to a civil transport aircraft could reduce operating costs by 7% and fuel burn by 11%.

Aerodynamic loads can be highly time dependent. If the load is assumed to vary sinusoidally, this can be expressed as a reduced frequency, k which can be as high as $k = 0.75 - 1$ for cruise conditions. Current alleviation strategies, such as ailerons, flaps and spoilers are unable to control these loads: their large inertia limits their frequency response. Advances in actuator technology [2] mean that control of aerodynamic loads at higher frequencies is now possible. Fluidic and mechanical actuators for load control have been proposed [3]. Control of dynamic loads was illustrated at low reduced frequencies for aeroelastic flutter suppression [4-6], while Andersen [7] and Heinz *et al* [8] investigated a mechanical device at higher frequencies. This paper examines a mechanical device, the mini-tab, examining its efficacy in a static configuration. This will be used to inform the design of a dynamic actuator.

1.1 Mini-tab Definition

The mini-tab is similar in principle to the Gurney flap, which has been investigated for airfoil lift increase. Both devices consist of a small tab placed perpendicularly to the airfoil surface. While the Gurney flap is placed on the lower surface close to the trailing edge to produce lift increase, the mini-tab is placed on the upper surface for lift decrease. Figure 1(a) illustrates the expected flow-field produced by an upper surface mini-tab. Flow should be separated close to the mini-tab location, reducing lift. Placement away from the trailing edge may prove to be preferable. As such, the present study investigates a variety of possible chordwise locations (see Fig. 1(b)).

1.2 Gurney Flap Literature

For small angles of attack and trailing-edge ($x_f/c = 1$) placement, symmetry can be used to compare the effects of the mini-tab and the Gurney flap even though the desired result is the opposite (lift decrease vs. increase). In a time-averaged sense, a region of separated flow is created behind the Gurney flap, producing a counter-rotating vortex pair [9-12]. This displaces the Kutta condition downstream of the trailing edge and increases the effective airfoil camber. The final part of the pressure recovery is completed off-surface, increasing suction over the upper surface. The changes in lift mean that the zero-lift angle, α_{0L} is reduced. When the angle of attack, α is increased,

the Gurney flap keeps the flow attached over the upper surface by increasing circulation close to the trailing edge. This increases c_{lmax} but decreases the stall angle. The drag penalty is small if the Gurney flap height is limited to less than the boundary layer thickness [13].

At the zero-lift angle, α_{0L}, the effect of upper and lower surface placement on the flow is similar, allowing for a common model to be used for the Gurney flap and mini-tab. Liu & Montefort [14] used thin airfoil theory to estimate the change in lift magnitude, $|\Delta c_l|$ as a function of the normalized tab height:

$$|\Delta c_l| = q\left(\frac{h}{c}\right)^{\frac{1}{2}} \qquad (1)$$

Where q is a parameter suggested by Liu & Montefort to be a function of Reynolds number, with values between 2 and 4.4 obtained for a variety of testing conditions. Additionally, Woods inviscid spoiler theory [15] considers a potential flow solution, suggesting a similar relationship. For a trailing edge location, the increment in lift coefficient is equal to:

$$|\Delta c_l| = 3.32\left(\frac{h}{c}\right)^{\frac{1}{2}} \qquad (2)$$

The square-root relationship has been compared to experiments [16-18] with a good agreement. In addition, linear empirical relationships based on the increase in circulation have been developed [19], however, these compare less favorably to the literature as a whole. Experiments [20] indicate that placement upstream of the trailing edge ($x_f/c \geq 0.90$) yields a smaller change in lift than placement directly at the trailing edge.

1.3 Mini-tab Literature

Compared to lower surface placement, research into upper surface mini-tabs for lift reduction is scarce. Yen-Nakafuji *et al* [21] demonstrated lift mitigation for upper surface placement close to the trailing edge, with a change in lift, Δc_l of up to -0.3. If treated like a trailing edge flap, the mini-tab's effect is expected to be constant with increasing α, however, a reducing $|\Delta c_l|$ was found by Baker *et al* [22]. Placement close to the trailing edge meant that the mini-tab was engulfed by the baseline flow separation as α increases.

Mini-tab placement upstream of the trailing edge may be superior for lift reduction across a wider range of angles of attack. In addition, the larger internal volume benefits the design of a movable actuator [23, 24]. Upper surface placement ahead of the trailing edge was studied by Baker *et al* [22] and Jacobs [25] for locations $x_f/c \geq 0.40$ and $x_f/c \leq 0.65$ respectively. The chordwise location has a significant effect on lift reduction, Δc_l and the lift curve slope, $c_{l\alpha}$. Baker *et al* [22] determined that, for small α, a mini-tab at $x_f/c = 0.60$ produced a more significant effect on c_l than trailing edge placement. Jacobs [25] found similar effects, with placement at $x_f/c = 0.65$ reducing c_{lmax} with no effect on $c_{l\alpha}$. Mini-tab placement at $x_f/c = 0.40$ [22] produced a small effect on c_l at $\alpha = 0°$ which

increased to stall. This reduced the lift curve slope, $c_{l\alpha}$. Leading edge placement (x_f/c = 0.05) [25] altered the lift curve significantly, with the largest effect at c_{lmax} producing $\Delta c_l \approx$ -1.0. Therefore, experiments indicate that the mini-tab's effects could be highly dependent on chordwise location, however, no study exists examining the full range of possible locations.

Woods theory [15] can model the effects of the mini-tab chordwise location, x_f/c on $|\Delta c_l|$ and $c_{l\alpha}$. Additionally, placement at the leading edge, x_f/c = 0 could be comparable to a flat plate with a leading edge flow separation, as studied theoretically by Kirchhoff [26] and Rayleigh [27] and experimentally by Fage & Johansen [28]. The pressure in the separated wake is assumed by both methods to be equal to the free-stream static value providing no contribution to lift.

1.4 Objectives

The mini-tab is a potential candidate technology for high frequency aerodynamic load control but, at present, the interdependence between its chordwise location, x_f/c, height, h/c and the airfoil angle of attack, α is poorly understood even for steady-state scenarios. This paper presents a comprehensive, experimental study of the mini-tab in a static or steady-state configuration to demonstrate this interdependence and explain the cause. These experiments are compared to theoretical models.

2. Experimental Apparatus & Procedures

2.1 Experimental Set-up

Force and Particle Image Velocimetry (PIV) measurements were conducted on a NACA0012 profile airfoil as shown in Fig. 1(b). The profile was selected due to its symmetric, generic profile and the wide range of data available in the literature with which to validate the current experiments. A chord length, c = 0.5 m and a span, b = 1.5 m were selected. The wing was mounted vertically within the test section of the University of Bath's large wind tunnel (illustrated in Fig. 2). The wind tunnel is a closed loop design with an octagonal test section of dimensions: 2.13 x 1.51 x 2.70 m. The span allowed for a small clearance of 5 mm or 0.3%b so that the wind tunnel walls could act as end plates effectively creating an infinite span, minimizing three dimensional effects. A free-stream velocity, U_∞ = 20 ms^{-1} was used throughout with a turbulent intensity measured as less than 0.5%U_∞. The model employs a boundary layer trip comprising a 0.3 mm diameter wire located at x/c = 0.10 on both surfaces as suggested by Pankhurst & Holder [29]. Barlow *et al* [30] indicate that this is the optimal location.

Two heights of mini-tab, h/c = 0.02 & 0.04, were constructed from carbon fiber in a simple "L"- shape with the root facing downstream. The mini-tab spanned the model with a thickness of 1.5 mm. The chordwise location of the mini-tab, x_f/c was varied between the positions shown in Fig. 1(b). At locations of x_f/c = 0.08, 0.60, 0.75,

0.85 and 0.95 the mini-tab was located in slots used for a parallel project involving spanwise blowing [31], which were covered when not in use. See [32] for more technical detail.

2.2 Force Measurements

The experimental parameters used for the initial force measurement survey are shown in Table 1. The airfoil was mounted from a bespoke two-component aluminum force balance, whose design has been previously used to good effect [33, 34]. The voltage output was conditioned and acquired using a Data Translation DAQ and a LabVIEW program, with 20,000 data-points acquired at a rate of 2 kHz. The force balance was aligned to measure forces parallel (*x*-axis) and perpendicular (*y*-axis) to the chord-line. Calibration of the force balance set-up was performed before each set of measurements using 30 known forces applied to the airfoil at the mid-span. To produce the required angle of attack, a stepper motor above the test section rotated both the airfoil and force balance. The measured forces were resolved to the flow direction. For the aerodynamic measurements, six repeats were performed per angle with the mean values presented. For the purposes of loads alleviation, the effect on lift is this paper's primary concern. Drag is less important and not presented here but it can be found in [32].

The force measurement technique's uncertainty was assessed using the methods of Moffat [35], see Table 1. Uncertainty in the force balance calibration coefficient was found to be 0.5%. The uncertainty in c_l was highest at stall, equaling ±0.013. Interference and blockage effects were evaluated using the methods of Pankhurst & Holder [29] and were found to have a small effect [32].

Table 1: Experimental parameters and the associated experimental uncertainties.

Parameter	Range or Value Considered	Uncertainty
***h/c*, mini-tab height**	0.02 to 0.04	±0.001
***x_f/c*, chordwise position**	0.08, 0.15, 0.30, 0.45, 0.60, 0.75, 0.85 & 0.95	±0.003
***Re*, Reynolds number**	6.6×10^5	$\pm 0.16 \times 10^5$
***α*, Angle of Attack**	-20° to 20°	±0.25°

2.3 Particle Image Velocimetry Measurements

From the initial force measurements, cases of interest were selected for further investigation using Particle Image Velocimetry (PIV), whose setup is shown in Fig. 2. The flow was seeded with olive oil via a six-jet TSI oil-droplet generator. The measurement plane was set normal to the airfoil surface at $z/b = 0.6$ to avoid reflections from pressure tappings located at the airfoil mid-span. The seeded flow was illuminated by a double pulsed 200 mJ 15 Hz Nd:YAG laser and captured using two four Megapixel TSI PowerView CCD cameras (2,048 x 2,048 pixels) with synchronization through a TSI LaserPulse synchronizer. Further measurements were performed at α

= 0° to include the downstream wake region. For these measurements, a pair of eight Megapixel TSI PowerView CCD cameras (3,312 x 2,488 pixels) were used to maintain vector resolution with an increased field-of-view.

To cover the full airfoil chord in a single set-up a "tandem" camera configuration was employed, see Fig. 2(b). The cameras were rotated with the airfoil as the angle of attack was altered to maintain the same view with a small overlap region. This created a total field of view of 0.6 m x 0.35 m (0.8 m x 0.35 m for the near wake measurements). As the mini-tab was placed on the airfoil upper surface, PIV measurements were only performed for the region above this surface. 400 image pairs were captured for each camera and processed using Insight 3G. The in-plane velocity vectors were calculated for each camera using a fast Fourier transform (FFT) cross-correlation algorithm between the image pairs. Interrogation windows of 24 x 24 pixels and 32 x 32 pixels were used for full chord and measurements including the wake respectively, producing an effective spatial resolution of 0.22%c. Instantaneous flow-field measurements are also presented to analyze the unsteady effects. The PIV measurements were acquired at 7.25 Hz and 2.5 Hz for 4 MP and 8 MP cameras respectively.

Post-processing of the velocity vectors was performed using MATLAB to merge the tandem data sets. A weighted average was applied in the overlap region between the cameras with a bias towards the image whose center was closest. The PIV uncertainty for the averaged flow-field was quantified as 1.25%U_∞ by combining the methods of Charonko & Vlachos [36] with those of Moffat [35]. The thickness of the plane of interest for the PIV measurements was of the order 2 mm, with an alignment error of ±1 mm.

3. Results & Discussion

3.1 Baseline Measurements

Figure 3 presents time-averaged lift coefficient, c_l vs. angle of attack, α, for the baseline NACA0012 airfoil without a mini-tab. The measurements are compared to thin airfoil theory along with a set of experimental measurements for a similar Reynolds number [37]. The two sets of experimental measurements compare well, with a similar lift curve slope, $c_{l\alpha}$ at both small angles of attack and close to stall. A stall angle of α = 13° is observed for both sets of measurements, with a c_{lmax} = 1.11 and 1.04 for [37] and the current measurements respectively. The review of NACA0012 data by McCroskey [38] indicates that this c_{lmax} value is comparable to the wider literature at this Reynolds number. Additionally, above α = 5° a deviation is observed between thin airfoil theory data and the two sets of experimental measurements. This reduction in gradient is indicative of a trailing edge flow separation that progresses towards the leading edge, termed by Gault [39] as "trailing edge stall". This is also validated in the PIV measurements shown later.

3.2 Force Measurements

Figure 4 presents force measurements for two mini-tab heights, h/c = 0.02 & 0.04 at the chordwise locations shown in Fig. 1(b). The mini-tab reduces lift in all configurations, however, the severity of lift reduction is highly dependent on the angle of attack, mini-tab height and chordwise location. In general, Figs. 4(a) and (b) indicate that lift reduction increases with increasing mini-tab height. The effect of the mini-tab employment can be observed more clearly by quantifying the change in lift between the baseline and mini-tab condition, Δc_l, as presented as a contour plot in Fig. 5.

Considering mini-tab location, placement near the trailing edge (x_f/c = 0.95) yields a high reduction in lift at α = 0°, with a reduction of up to Δc_l = -0.48 for a height of h/c = 0.04. As the angle of attack increases towards stall, lift reduction diminishes. This has been noted previously by Baker *et al* [22]. This equates to an increase in $c_{l\alpha}$ when compared to the baseline case as shown in Fig. 4 for x_f/c = 0.95.

Moving the mini-tab forwards from the trailing edge, to x_f/c = 0.85 and 0.75, reduces effectiveness at α = 0° consistent with the effects noted by Li *et al* [20]. An increase in $c_{l\alpha}$ is noted but it is less severe than placement closer to the trailing edge. As with x_f/c = 0.95, a reduction in effectiveness is observed as the angle of attack approaches stall.

In contrast, lift reduction at α = 0° is increased for x_f/c = 0.60 when compared to x_f/c = 0.95. For example, a mini-tab height of h/c = 0.04 increases lift reduction from Δc_l = -0.48 at x_f/c = 0.95 to Δc_l = -0.60 at x_f/c = 0.60. Moreover, this location produces a more uniform reduction in lift across small angles of incidence (0° ≤ α ≤ 5°) as indicated in Fig. 5 by a uniform Δc_l. The lift curve slope between these angles is equal to that of the baseline airfoil. As α increases, Fig. 5 shows the lift mitigation reducing for x_f/c = 0.60, like x_f/c = 0.95, however, the mid-chord location still reduces lift at baseline stall (α = 13°), with a lift reduction of Δc_l = -0.14 and -0.34 achievable for mini-tab heights, h/c = 0.02 and 0.04 respectively.

Mini-tab placement near the leading edge (x_f/c = 0.08) produces a different effect. It is noted that this location is ahead of the transition wire location. Figure 4 indicates that a minimal effect is observed at α = 0°, with Δc_l = -0.03 and -0.04 for h/c = 0.02 and 0.04 respectfully. When α is increased, there is a sudden and significant change in lift curve slope, $c_{l\alpha}$. This occurs at different angles for the different heights of mini-tab: $\alpha \approx 4°$ and 0° for h/c = 0.02 and 0.04 respectively. This means that c_l at stall is significantly reduced: -0.47 and -0.67 for h/c = 0.02 and 0.04 respectively. A hypothesis for this effect is presented in section 3.4.

Figure 5 indicates a transition in the effect on Δc_l between $x_f/c = 0.60$ and $x_f/c = 0.08$ from the mini-tab having its largest effect at small α to a greater efficacy at stall. This suggests that the position for maximum lift reduction is highly dependent on α, moving from the trailing edge to the leading edge as the angle increases.

3.3 Comparison to Theoretical Models

As previously described, the change in lift at $\alpha = 0°$ can be estimated using the methods of Liu & Montefort [14] and Woods [15]. Figure 6 presents a comparison of the two theories to the present measurements and those from literature for symmetric [10, 12, 14, 20] and cambered airfoils [11, 22, 40-42]. In order to reduce any effects of airfoil camber, the magnitude of the change in lift is considered for the airfoil zero lift angle, $|\Delta c_l|_{REF,\, L\,=\,0}$. As the NACA0012 profile is symmetric, this value should be equal for upper and lower surface placement at $\alpha = 0°$. The comparison is limited to data obtained with the device close to the trailing edge ($x_f/c \geq 0.95$), to minimize the effect of chordwise location. The NACA0012 airfoil data is denoted by solid symbols. In addition to the two theories, a simple curve fit is applied in the form of:

$$|\Delta c_l|_{REF,\, L=0} = q \times \left(\frac{h}{c}\right)^n \qquad (3)$$

This is a modification of equations 1 and 2, where both q and n are allowed to vary freely. Previously, n was suggested by both Liu & Montefort [14] and Woods [15] to be 0.5, however, it has been noted by Greenwell [19] that this value may be closer to 0.7. Liu & Montefort suggest that q is a parameter dependent on Reynolds number and airfoil profile, whereas Woods fixes this value at 3.32.

Analyzing Fig. 6, a clear trend is observed. As one would expect $|\Delta c_l|_{REF,L\,=\,0}$ increases with increasing mini-tab height. The quality of theoretical fit is quantified by the coefficient of determination, R^2. This equals 0.54 for the theory of Liu & Montefort [14] using a fixed n of 0.5. The fit's quality is improved slightly by the introduction of a variable n parameter, increasing from 0.5 to 0.63. This increase is consistent with the conclusions of Greenwell [19]. In addition, the inviscid theory of Woods [15] dramatically overpredicts the change in lift, with a q factor of 3.32 opposed to 2.27 for the theory of Liu & Montefort [14] and poorly fits the data with $R^2 = 0.16$. It may be suggested that this lower q value could be linked to the difference in the theoretical formulations. Liu & Montefort introduce a variable q parameter, which appears to act as an empirical correction. This may account for viscous effects arising in the boundary layer which reduces the velocity close to the surface. The results obtained in the current study lie close to both the theory of Liu & Montefort and the curve fit, and clearly within the range of previous measurements.

In section 3.2, a severe reduction in lift curve slope was noted when the mini-tab is located near the leading edge ($x_f/c = 0.08$). Figure 7 presents lift coefficient for the two mini-tab heights, $h/c = 0.02$ and 0.04, alongside

the theory of Kirchhoff [26] and Rayleigh [27]. The lift coefficient for a flat plate with a leading edge flow separation is reported by Wick [43] as:

$$c_l = \frac{2\pi \sin\alpha}{4+\pi \sin\alpha}\cos\alpha \qquad (4)$$

While this relationship represents a fully separated flow, it suggests a good agreement for a mini-tab of normalized height, h/c = 0.04 between α = 0° and 7° and agrees with gradient of the h/c = 0.02 case between 3° < α < 8°. This suggests that the flow is fully separated, a hypothesis which will be investigated in Section 3.4 using PIV.

Woods inviscid spoiler theory [15] expresses the change in lift at α = 0° as function of the mini-tab chordwise location, x_f/c and mini-tab height, h/c. This is presented as equation 5 and is plotted in Fig. 8(a) alongside the change in lift at α = 0° for all locations and heights, denoted as $|\Delta c_l|_{\alpha=0}$.

$$|\Delta c_l|_{\alpha=0} = \frac{0.749\pi}{2}\left(1+\sqrt{x_f/c}\right)^2\left(\frac{h/c}{x_f/c+\sqrt{x_f/c}}\right)^{\frac{1}{2}}\left(1-\frac{1-\sqrt{x_f/c}}{1+\sqrt{x_f/c}}\right) \qquad (5)$$

Both mini-tab heights indicate that $|\Delta c_l|_{\alpha=0}$ decreases as the mini-tab towards the leading edge. Between x_f/c = 0.95 and 0.60, the effects for the two mini-tab heights differ slightly. The mini-tab of height, h/c = 0.04 produces an increase in $|\Delta c_l|_{\alpha=0}$ as it is moved forward, whereas the effect for h/c = 0.02 remains approximately constant. In addition, Woods inviscid spoiler theory presents a similar trend as the experimental results, with a decreasing effect towards the leading edge albeit with $|\Delta c_l|_{\alpha=0}$ overpredicted. The overprediction may be due once again to the effect of the boundary layer reducing the mini-tab's efficacy, which is not predicted by the theory.

The theory of Woods [15] can also be used to estimate the mini-tab's effect on the lift curve gradient, $c_{l\alpha}$ as shown in equation 6:

$$c_{l\alpha} = \frac{\pi}{2}\left(1+\sqrt{x_f/c}\right)^2 \qquad (6)$$

It is important to note that equation 6 suggests that the effect on $c_{l\alpha}$ is only a function of the chordwise location and not the mini-tab height. Using this equation, placement at x_f/c = 0 yields a gradient of $\pi/2$ per radian: identical to Kirchhoff [26] and Rayleigh [27] prediction, and the gradient for trailing edge placement is the same as that produced by thin airfoil theory: 2π per radian. Figure 8(b) compares this relationship to experimental data at α = 0°, where the gradient was calculated using central differencing. The gradient is normalized in each case by the baseline gradient, $c_{l\alpha,REF}$ which was determined for the experimental measurements as 2.04π per radian. The experimental results of Jacobs [25] are also added for a mini-tab of height, h/c = 0.0125.

In general, the theoretical relationship of Woods [15] captures the trend very well for h/c = 0.0125 (from Jacobs [25]), 0.02 and 0.04 with $x_f/c \geq 0.3$, with an underestimation of the gradient noticeable for mini-tab locations close to the trailing edge. For $x_f/c < 0.3$, a large disparity in $[c_{l\alpha}/c_{l\alpha, REF}]_{\alpha = 0}$ is observed between different mini-tab heights. At x_f/c = 0.08, a mini-tab of height, h/c = 0.02 appears to return to the baseline gradient, whereas h/c = 0.04 shows a prodigious decrease in $[c_{l\alpha}/c_{l\alpha, REF}]_{\alpha = 0}$. The reasons for this difference relate to the separation and reattachment of flow, and are explained in section 3.4.

3.4 Particle Image Velocimetry Measurements

Using the time-averaged flow-field measurements, the cause of the change in time-averaged lift can be investigated. Figures 9 and 10 show time-averaged velocity magnitude and streamlines for cases involving mini-tab heights, h/c = 0.02 and 0.04 respectively. The PIV measurements are divided into four columns (baseline and x_f/c = 0.08, 0.60 and 0.95), along with five rows representing the angles of attack (α = 0°, 5°, 8°, 10° and 13°). These angles are also highlighted in red on the c_l-α curve at the top of the figure.

The flow-field presented in Fig. 9 for x_f/c=0.95 and α = 0° indicates that the effect on the flow is similar to that for conventional Gurney flap. For h/c = 0.02, a small separation region occurs behind the mini-tab. As suggested by literature [16], this causes a shift in the Kutta condition into the downstream wake region. An increase in mini-tab height to h/c = 0.04 increases the size of the flow separation (see Fig. 10). The separated region causes an effective negative camber producing a reduction in lift which increases with mini-tab height.

For the baseline configuration, increasing α causes flow separation to develop on the airfoil upper surface. For x_f/c = 0.95, the time-averaged velocity fields presented in Figs. 9 and 10 indicate that the flow separation progresses ahead of the mini-tab location as α increases. For the baseline airfoil, stall occurs around α = 13°. Fig. 9 indicates that at this angle the h/c = 0.02 mini-tab is fully immersed in the separated flow. This reduces its efficacy, as hypothesized by Baker *et al* [22]. In contrast, h/c = 0.04 (Fig. 10) retains some effectiveness at the high angles of incidence. At α = 13°, a small lift reduction is noted (Δc_l = -0.15) because the larger mini-tab can displace the shear layer away from the airfoil surface.

Positioning the mini-tab towards the mid-chord at x_f/c = 0.60 produced a consistent effect from α = 0° to 5°. The flow-field measurements for α = 0° indicate a large flow separation behind the mini-tab which is maintained beyond the trailing edge for both mini-tab heights. Between α = 8° and 13° this location clearly advances the separation ahead of the baseline location. At α =13°, a portion of separated flow is observed ahead of the mini-tab location, with the mini-tab of height, h/c = 0.02 becoming almost fully immersed within the separated wake region. However, for both heights the flow separation enlarged in comparison to the baseline and the separation

point moved towards the leading edge. Hence, the mini-tab continues to be effective, with Δc_l = -0.35 achievable for the h/c = 0.04 mini-tab.

Close to the leading edge (x_f/c = 0.08), the flow-field is highly dependent on the mini-tab height. Figure 9 indicates that the mini-tab separates the flow close to its location which then reattaches close to the mid-chord. In contrast, the h/c = 0.04 mini-tab (Fig. 10) induces a flow separation which, much like the x_f/c = 0.60 location, does not reattach. Comparison of the PIV and lift coefficient measurements indicates that even though the flow is separated, partially and fully for h/c = 0.02 and 0.04 respectively, neither configuration produces a significant reduction in lift (Δc_l = -0.03 and -0.04 for h/c = 0.02 and 0.04 respectfully). Surface pressure measurements (see [32, 44]) show that the increased suction caused by the higher velocity flow over the lower surface is balanced by the effects of stagnation ahead and separation of the flow behind the mini-tab resulting in no significant difference in the lift estimated through the integration of the pressure field.

As indicated in Fig. 8, there is a significant effect on the gradient at α = 0° which is dependent on the mini-tab height. For the larger mini-tab (h/c = 0.04) the gradient changed in agreement with Woods spoiler theory [15], whereas, for the smaller heights (h/c = 0.02 and 0.0125 from Jacobs [25]) the flow reattached with the gradient more comparable to the baseline condition. The discontinuity in lift curve gradient can be described by considering laminar separation bubbles (which are not present in the baseline flow) close to the leading edge of the airfoil, using the definitions laid out by Tani [45] and comparing their attributes to the mini-tab induced separation. In principle, the flow condition created by the mini-tab is similar to that created during thin airfoil stall. A "short" separation bubble, as shown at α = 0° only has a small effect on the lift coefficient. As the angle of attack is increased, the "short" separation bubble steadily grows with the reattachment point moving towards the trailing edge. Eventually, the reattachment point reaches the airfoil trailing edge and the bubble does not reattach, becoming a detached flow separation. The lift coefficient measurements for h/c = 0.02 in Fig. 7, indicate that this "bursting" occurs at $\alpha \approx 3°$ and the flow-field at α = 5° clearly show a fully separated flow in support of this hypothesis. In this fully separated condition, the mini-tab has a significant effect on lift coefficient, efficiently mitigating suction over the upper surface producing a significant reduction in $c_{l\alpha}$. This is supported by pressure measurements [32, 44].

3.5 Unsteady Forces and Instantaneous Flow-fields

The standard deviation of lift coefficient is presented in Fig. 11(a) for the baseline and three mini-tab locations: x_f/c = 0.08, 0.60 and 0.95. In addition, instantaneous flow-field measurements are presented in Figs. 11(b) and (c)

to examine the unsteady aspects produced by the mini-tab on the flow-field for x_f/c = 0.08 and 0.60 for α = 0°, 5° and 8°. While only a single flow-field is presented, these measurements are representative of the unsteady flow.

Firstly, the baseline, clean configuration is considered. The standard deviation of lift coefficient, σ_{cl} increases towards stall, beyond which unsteadiness increases dramatically. The large σ_{cl} at α = 13° is consistent with the highly unsteady flow expected at stall. When trailing edge placement (x_f/c = 0.95) is compared to the baseline measurements, there appears to be a minimal change in the unsteady forces. This is the case across all angles of attack. It has been previously discovered [46] that the mini-tab produces a von Karman vortex street for locations close to the trailing edge. This suggests an unsteadiness in the flow which is not present in the force measurements. As the mini-tab is placed close to the trailing edge the unsteadiness acts over a small proportion of the upper surface which may have a small effect on lift.

Locating the mini-tab at x_f/c = 0.60 increased the standard deviation in lift at α = 0° to σ_{cl} = 0.015. Flow-field measurements presented in Fig. 11(b) indicate an unsteady separated region that extends beyond the trailing edge. Increasing the angle of attack produces a decrease in the measured unsteadiness and σ_{cl} returns to the baseline condition at $\alpha \approx 5°$. At α = 5° and 8° the unsteady shear layer is displaced further away from the airfoil surface, reducing its influence on σ_{cl}.

The x_f/c = 0.08 mini-tab produced the opposite trend in σ_{cl} compared to the two other locations. In comparison to the baseline flow, no change is observed at α = 0°. Analysis of the measurements at α = 0° (Fig. 11(c)) suggest that the separated shear layer is close to the surface, with only small strwuctures present in the flow and the streamlines at the trailing edge only slightly perturbed. It is suggested that the small perturbations produce a minimal effect on $\sigma_{cl.}$ As the angle increases the unsteadiness rapidly rises to σ_{cl} = 0.05 at α = 5° and then plateaus until stall. At α = 5° and 8°, the flow-field measurements indicate the presence of larger unsteady structures behind the mini-tab. It is suggested that the scale of the structures, coupled to their small distance from the upper surface, increases the unsteady forces.

4. Conclusions

An experimental investigation was conducted on a NACA0012 airfoil equipped with upper surface mini-tabs, to investigate the feasibility of mini-tabs for load control. In general, greater lift reduction was found for larger mini-tabs. Locating the mini-tab close to the trailing edge (x_f/c = 0.95) produces a significant lift reduction for small angles of attack, α. As α is increased, the mini-tab becomes immersed in the airfoil's baseline flow separation and becomes ineffective near stall. In comparison, the large flow separation induced by the mini-tab at x_f/c = 0.60 reduces lift effectively at a wide range of angles of attack. At this location, the mini-tab is positioned far enough

forward to advance flow separation at angles of attack close to stall. Locating the smaller mini-tab close to the leading edge produces a minimal effect at $\alpha = 0°$ where flow reattachment eliminates any effect. At higher angles of attack, the bubble bursts creating a fully separated flow and therefore produces an increasing lift reduction towards stall. Changes in the lift curve slope compare well with the theory, as long as there is no reattachment. Analysis of the unsteady force and instantaneous flow-field measurements indicate an increase in the standard deviation of lift coefficient for $x_f/c = 0.08$, where the presence of a highly unsteady shear layer close to the airfoil surface provides a greater source of unsteadiness.

Acknowledgments

The authors would like to thank Airbus UK for the financial support supplied to this project. A University Research Studentship from the University of Bath supported the author's work. The project was also assisted by EPSRC strategic equipment grant (EP/K040391/1 & EP/M000559/1) and EPSRC project (EP/M022307/1).

References

1. Xu, J., and Kroo, I. "Aircraft Design with Active Load Alleviation and Natural Laminar Flow," *Journal of Aircraft,* Vol. 51, No. 5, 2014, pp. 1532-1545.
2. Cattafesta III, L. N., and Sheplak, M. "Actuators For Active Flow Control," *Annual Review of Fluid Mechanics,* Vol. 43, 2011, pp. 247-272.
3. Blaylock, M., Chow, R., Cooperman, A., and van Dam, C. P. "Comparison of Pneumatic Jets and Tabs for Active Aerodynamic Load Control," *Wind Energy,* Vol. 17, No. 9, 2014, pp. 1365-1384.
4. Bieniawski, S., Kroo, I., and Wolpert, D., "Flight Control with Distributed Effectors," *AIAA Guidance, Navigation, and Control Conference and Exhibit,* AIAA-2005-6074, AIAA, San Fransisco, 2005.
5. Lee, H.-T., and Kroo, I., "Computational Investigation of Airfoils with Miniature Trailing Edge Control Surfaces," *42nd AIAA Aerospace Sciences Meeting and Exhibit,* AIAA-2004-1051, AIAA, Reno, 2004.
6. Bieniawski, S., and Kroo, I., "Development and Testing of an Experimental Aeroelastic Model with Micro-Trailing Edge Effectors," *41st Aerospace Sciences Meeting and Exhibit,* AIAA-2003-0220, AIAA, Reno, 2003.
7. Andersen, P. B., "Advanced Load Alleviation for Wind Turbines using Adaptive Trailing Edge Flaps: Sensoring and Control," PhD Thesis, Technical University of Denmark, 2010.
8. Heinz, J., Sørensen, N. N., and Zahle, F. "Investigation of the load reduction potential of two trailing edge flap controls using CFD," *Wind Energy,* Vol. 14, No. 3, 2011, pp. 449-462.
9. Liebeck, R. H. "Design of Subsonic Airfoils for High Lift," *Journal of Aircraft,* Vol. 15, No. 9, 1978, pp. 547-561.
10. Gai, S. L., and Palfrey, R. "Influence of Trailing-Edge Flow Control on Airfoil Performance," *Journal of Aircraft,* Vol. 40, No. 2, 2003, pp. 332-337.
11. Myose, R., Papadakis, M., and Heron, I. "Gurney Flap Experiments on Airfoils, Wings, and Reflection Plane Model," *Journal of Aircraft,* Vol. 35, No. 2, 1998, pp. 206-211.
12. Date, J. C., and Turnock, S. R. "Computational Evaluation of the Periodic Oerformance of a NACA 0012 Fitted with a Gurney Flap," *Journal of Fluids Engineering,* Vol. 124, No. 1, 2002, pp. 227-234.
13. Brown, L., and Fillipone, A. "Aerofoil At Low Speeds With Gurney Flaps," *Aeronautical Journal,* Vol. 107, No. 1075, 2003, pp. 539-546.
14. Liu, T., and Montefort, J. "Thin-Airfoil Theoretical Interpretation for Gurney Flap Lift Enhancement," *Journal of Aircraft,* Vol. 44, No. 2, 2007, pp. 667-671.
15. Woods, L. C. *The Theory of Subsonic Plane Flow,* Cambridge University Press, 1961.
16. Feng, L.-H., Jukes, T. N., Choi, K.-S., and Wang, J.-J. "Flow Control Over a NACA 0012 Airfoil Using Dielectric-Barrier-Discharge Plasma Actuator with a Gurney Flap," *Experiments in Fluids,* Vol. 52, No. 6, 2012, pp. 1533-1546.

17. Libin, D., and Traub, L. W. "Effect of Aspect Ratio on Gurney-Flap Performance," *Journal of Aircraft*, Vol. 50, No. 4, 2013, pp. 1217-1225.

18. Yu, T., Wang, J. J., and Zhang, P. F. "Numerical Simulation of Gurney Flap on RAE-2822 Supercritical Airfoil," *Journal of Aircraft*, Vol. 48, No. 5, 2011, pp. 1565-1575.

19. Greenwell, D. I. "Gurney Flaps on Slender and Nonslender Delta Wings," *Journal of Aircraft*, Vol. 47, No. 2, 2010, pp. 675-681.

20. Li, Y., Wang, J., and Zhang, P. "Influences of Mounting Angles and Locations on the Effects of Gurney Flaps," *Journal of Aircraft*, Vol. 40, No. 3, 2003, pp. 494-498.

21. Yen Nakafuji, D. T., van Dam, C. P., Michel, J., and Morrison, P., "Load Control for Turbine Blades: A Non-Traditional Microtab Approach," *ASME 2002 Wind Energy Symposium*, ASME, Reno, Year.

22. Baker, J. P., Standish, K. J., and Van Dam, C. P. "Two-Dimensional Wind Tunnel and Computational Investigation of a Microtab Modified Airfoil," *Journal of Aircraft*, Vol. 44, No. 2, 2007, pp. 563-572.

23. Cooperman, A. M., Chow, R., and van Dam, C. P. "Active Load Control of a Wind Turbine Airfoil Using Microtabs," *Journal of Aircraft*, Vol. 50, No. 4, 2013, pp. 1150-1158.

24. Tang, D., and Dowell, E. H. "Aerodynamic Loading for an Airfoil with an Oscillating Gurney Flap," *Journal of Aircraft*, Vol. 44, No. 4, 2007, pp. 1245-1257.

25. Jacobs, E. N. "Airfoil Section Characteristics as Affected by Protuberances." NACA Technical Report No. 446, 1934.

26. Kirchhoff, G. "Zur Theorie freier Flüssigkeitsstrahlen," *Journal für die Reine und Angewandte Mathematik*, Vol. 70, 1869, pp. 289-298.

27. Rayleigh, L. "Notes on hydrodynamics," *The London, Edinburgh, and Dublin Philosophical Magazine and Journal of Science*, Vol. 2, No. 13, 1876, pp. 441-447.

28. Fage, A., and Johansen, F. C. "On the Flow of Air behind an Inclined Flat Plate of Infinite Span," *Proceedings of the Royal Society of London A: Mathematical, Physical and Engineering Sciences*, Vol. 116, No. 773, 1927, pp. 170-197.

29. Pankhurst, R. C., and Holder, D. W. *Wind-Tunnel Technique: An Account of Experimental Methods in Low-and High-Speed Wind Tunnels*, London, Pitman, 1952.

30. Barlow, J., Rae, W., and Pope, A. *Low-Speed Wind Tunnel Testing*, 1999.

31. Al Battal, N., Cleaver, D. J., and Gursul, I., "Aerodynamic Load Control through Blowing," *54th AIAA Aerospace Sciences Meeting*, AIAA-2016-1820, AIAA, San Diego, 2016.

32. Heathcote, D. J., "Mini-tabs for Aerodynamic Loads Alleviation," PhD Thesis, Unversity of Bath, 2017.

33. Gursul, I., Cleaver, D., and Wang, Z. "Control of Low Reynolds Number Flows by Means of Fluid–Structure Interactions," *Progress in Aerospace Sciences*, Vol. 64, 2014, pp. 17-55.

34. Cleaver, D. J., Wang, Z., Gursul, I., and Visbal, M. "Lift Enhancement by Means of Small-Amplitude Airfoil Oscillations at Low Reynolds Numbers," *AIAA Journal*, Vol. 49, No. 9, 2011, pp. 2018-2033.

35. Moffat, R. J. "Describing The Uncertainties in Experimental Results," *Experimental Thermal and Fluid Science*, Vol. 1, No. 1, 1988, pp. 3-17.

36. Charonko, J. J., and Vlachos, P. P. "Estimation of Uncertainty Bounds For Individual Particle Image Velocimetry Measurements From Cross-Correlation Peak Ratio," *Measurement Science and Technology*, Vol. 24, No. 6, 2013, p. 065301.

37. Jacobs, E. N., and Sherman, A. "Airfoil section characteristics as affected by variations of the Reynolds number." NACA Technical Report No. 586, 1937.

38. McCroskey, W. "A Critical Assessment of Wind Tunnel Results For The NACA 0012 Airfoil." NASA Technical Memorandum 100019, 1987.

39. Gault, D. E. "A Correlation of Low-Speed, Airfoil-Section Stalling Characteristics With Reynolds Number and Airfoil Geometry." NACA Technical Note No. 3963, 1957.

40. Storms, B., and Jang, C. S., "Lift Enhancement of an Airfoil using a Gurney Flap and Vortex Generators," *31st Aerospace Sciences Meeting*, AIAA-1993-0647, AIAA, 1993.

41. Maughmer, M. D., and Bramesfeld, G. "Experimental investigation of Gurney Flaps," *Journal of Aircraft*, Vol. 45, No. 6, 2008, pp. 2062-2067.

42. Nakafuji, D. Y., Van Dam, C., Smith, R., and Collins, S. "Active Load Control For Airfoils Using Microtabs," *Journal of Solar Energy Engineering*, Vol. 123, No. 4, 2001, pp. 282-289.

43. Wick, B. H. "Study of the Subsonic Forces and Moments on an Inclined Plate of Infinite Span." NACA Technical Note 3221, 1954.

44. Heathcote, D. J., Gursul, I., and Cleaver, D. J., "An Experimental Study of Mini-Tabs for Aerodynamic Load Control," *54th AIAA Aerospace Sciences Meeting*, AIAA-2016-0325, AIAA, San Diego, 2016.

45. Tani, I. "Low-Speed Flows involving Bubble Separations," *Progress in Aerospace Sciences*, Vol. 5, 1964, pp. 70-103.

46. Lee, T., and Ko, L. "PIV Investigation of Flowfield Behind Perforated Gurney-Type Flaps," *Experiments in Fluids*, Vol. 46, No. 6, 2009, pp. 1005-1019.

Figures

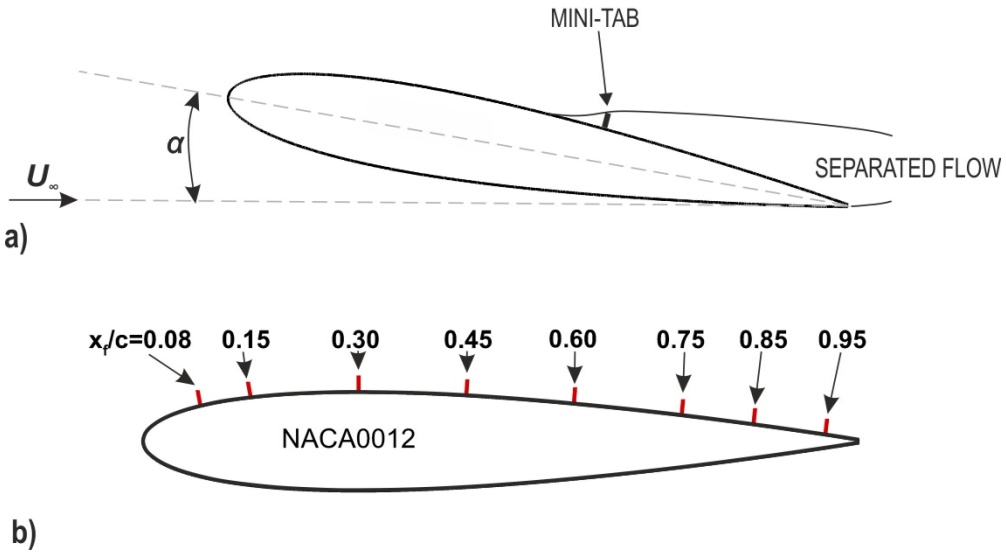

Figure 1: (a) Illustration of flow-field created by an upper surface mini-tab, (b) Schematic of mini-tab locations used for experiments.

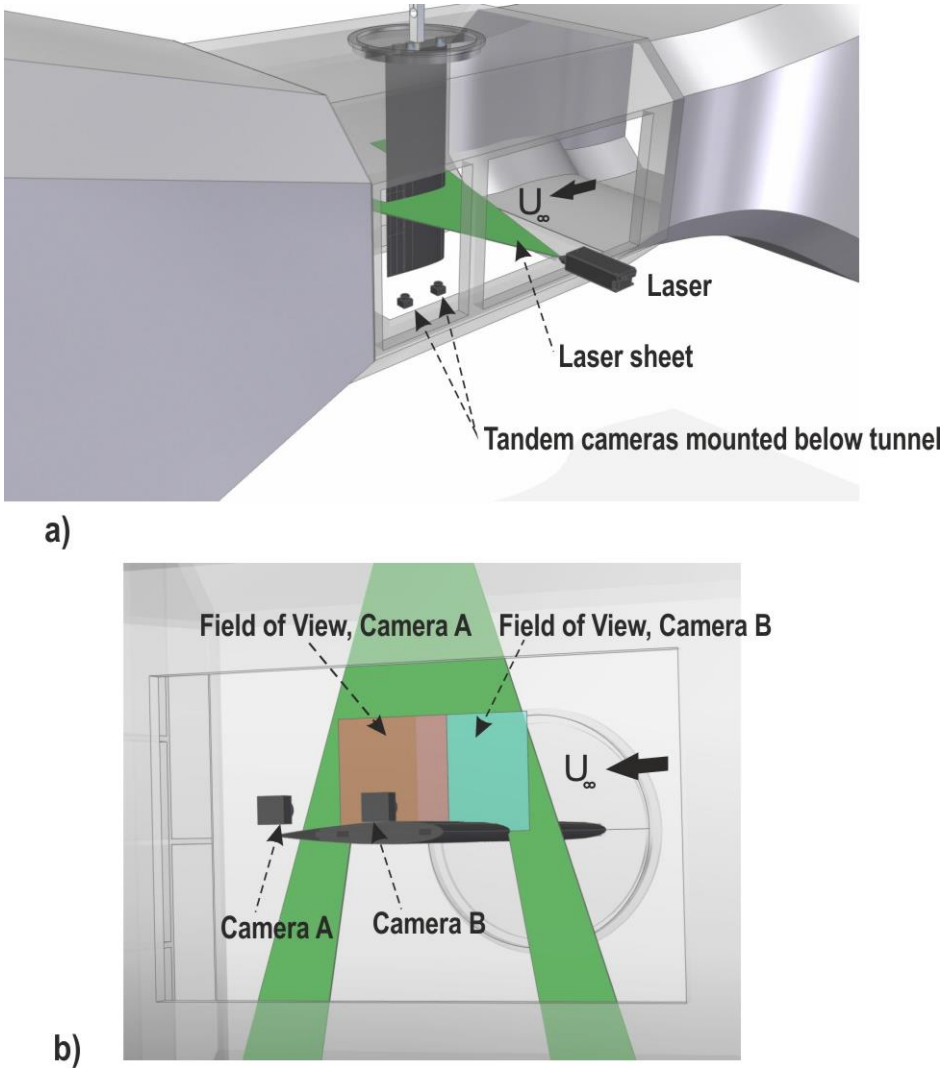

Figure 2: Experimental set-up for Particle Image Velocimetry measurements shown (a) from the side and (b) from below highlighting the fields of view of the tandem cameras.

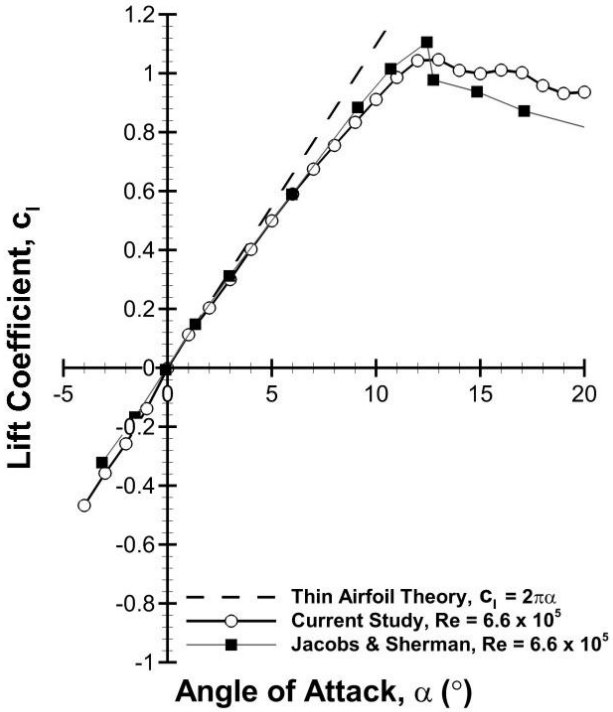

Figure 3: Comparison of baseline lift coefficient vs. angle of attack to thin airfoil theory and existing literature [37] at a comparable Reynolds number.

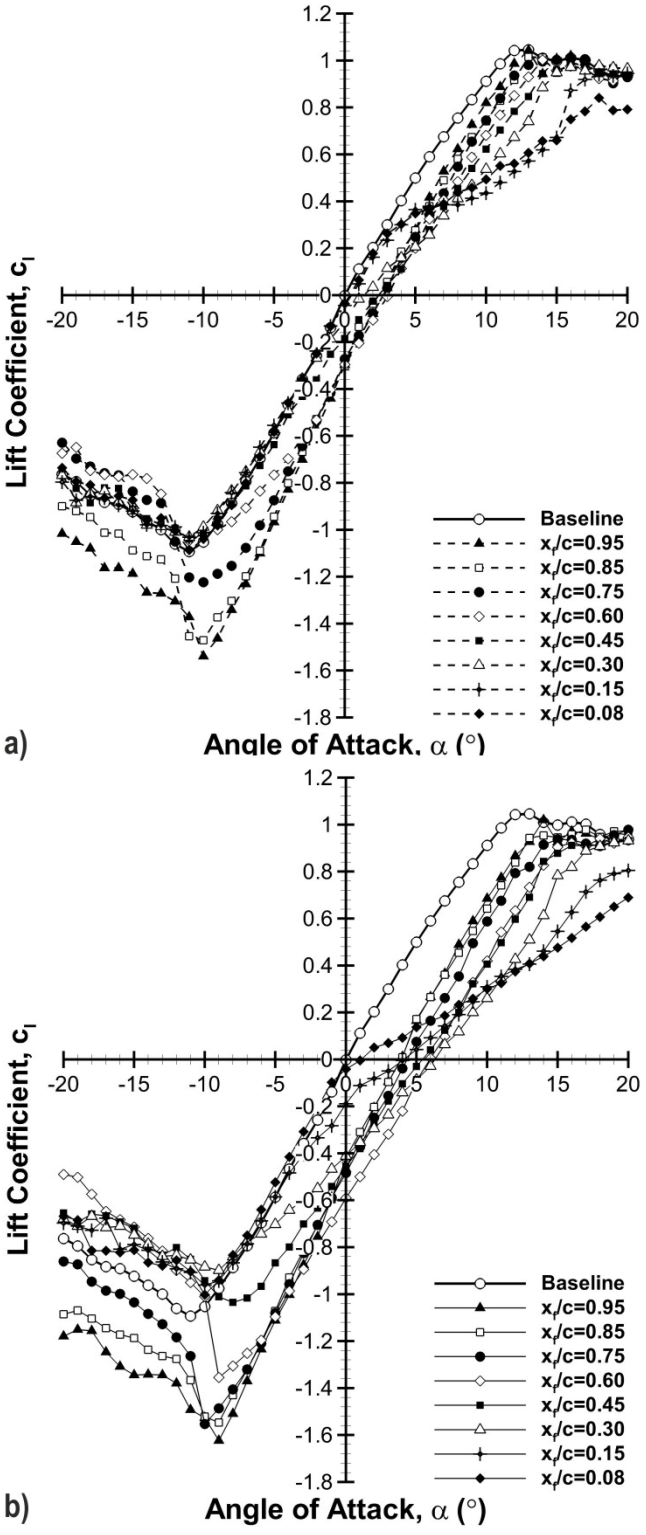

Figure 4: Time-averaged lift coefficient, c_l vs. angle of attack for heights, (a) h/c = 0.02 & (b) 0.04.

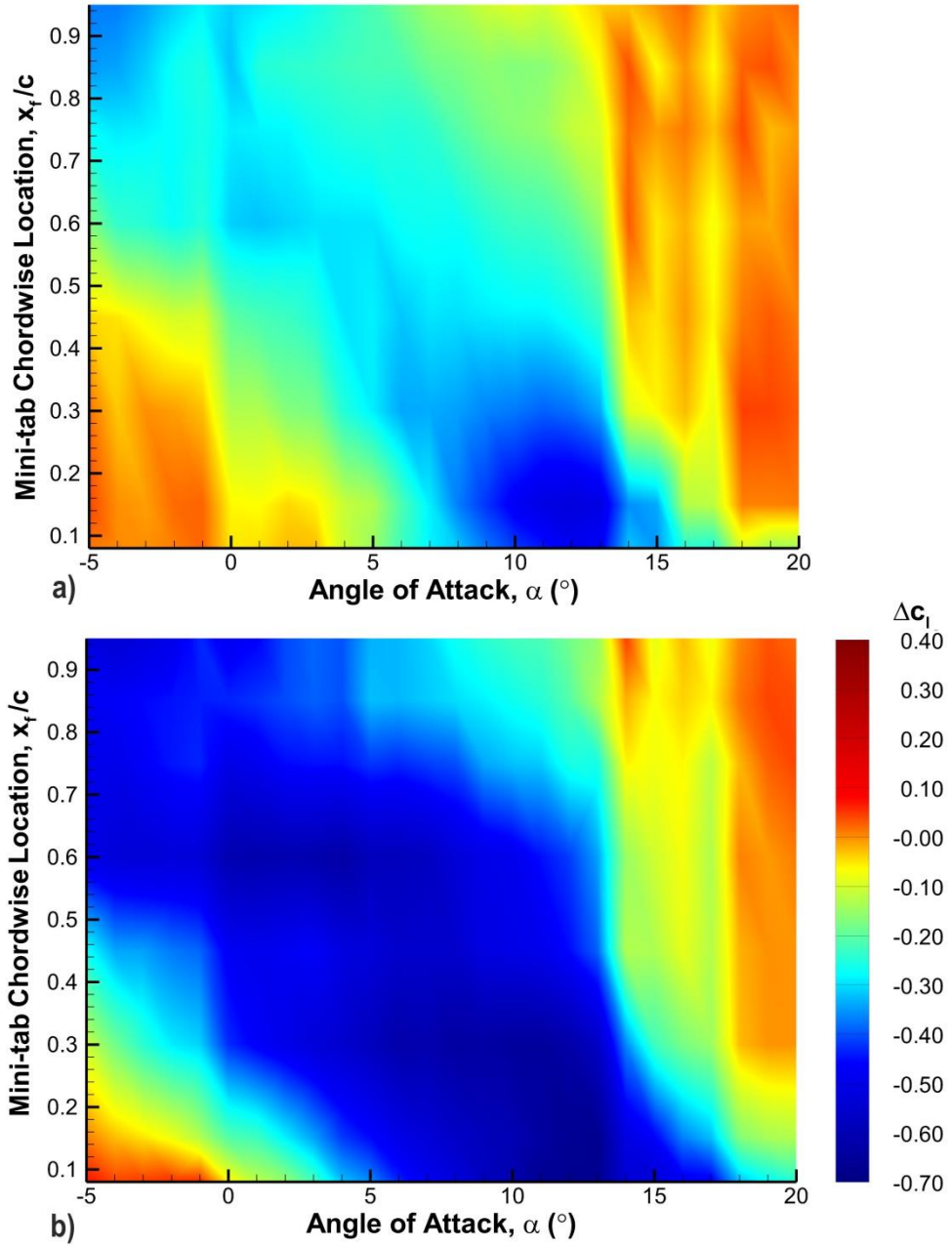

Figure 5: Contour plots presenting the change in time-averaged lift coefficient (Δc_l) as a function of chordwise location and angle of attack for mini-tabs of height, (a) h/c = 0.02 & (b) h/c = 0.04.

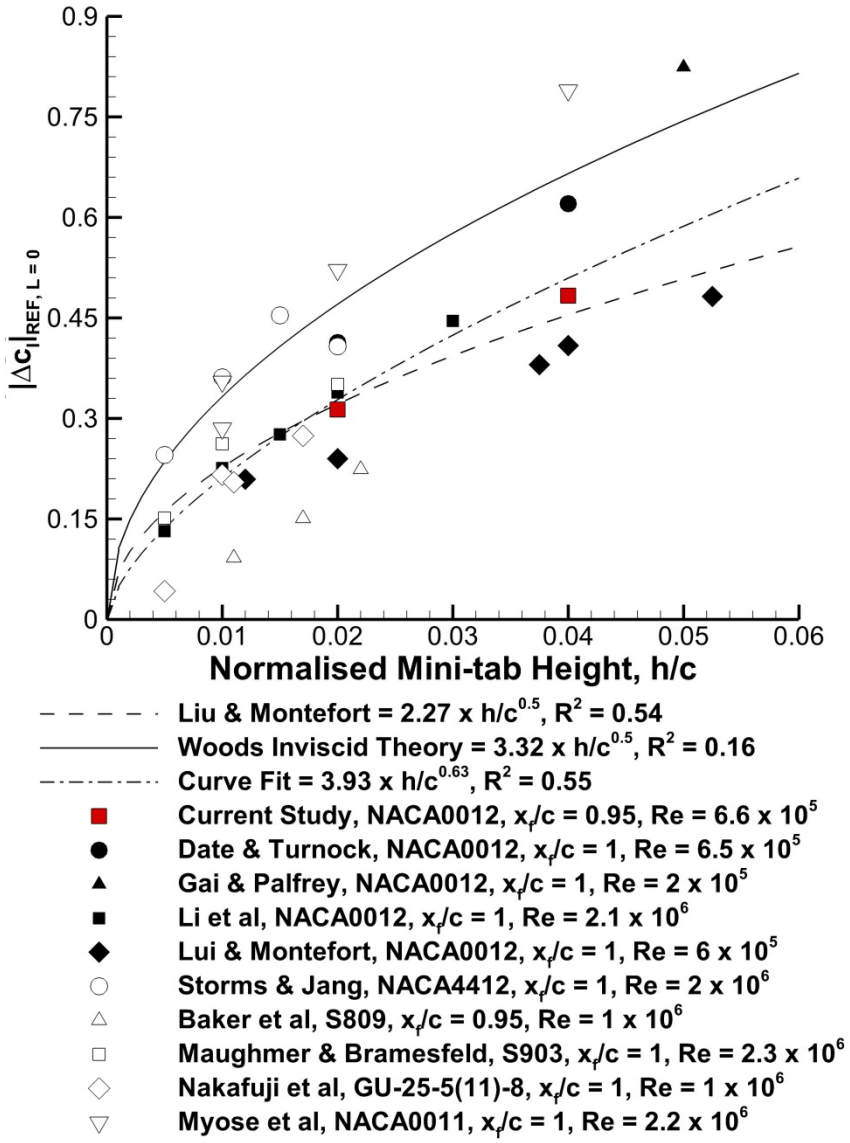

Figure 6: Magnitude of change in lift at zero lift angle ($|\Delta c_l|_{REF, L = 0}$) as a function of mini-tab height for (a) all airfoil profiles and (b) NACA0012 profiles only. Trend lines illustrate Liu and Montefort [14] method with a simple curve fit and Woods [15] inviscid spoiler theory.

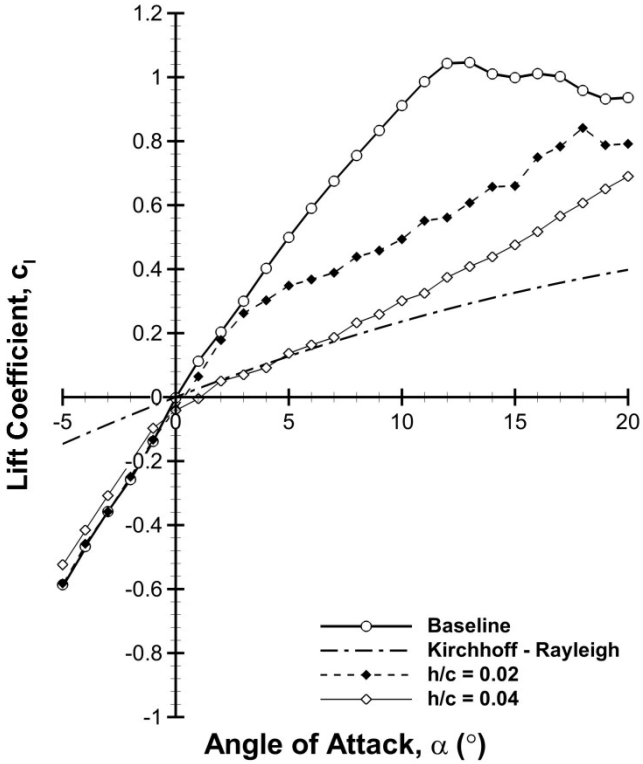

Figure 7: Comparison of lift coefficient vs. angle of attack for x_f/c = 0.08. A comparison to Kirchhoff-Rayleigh [26, 27] theory for inviscid separated flow is provided.

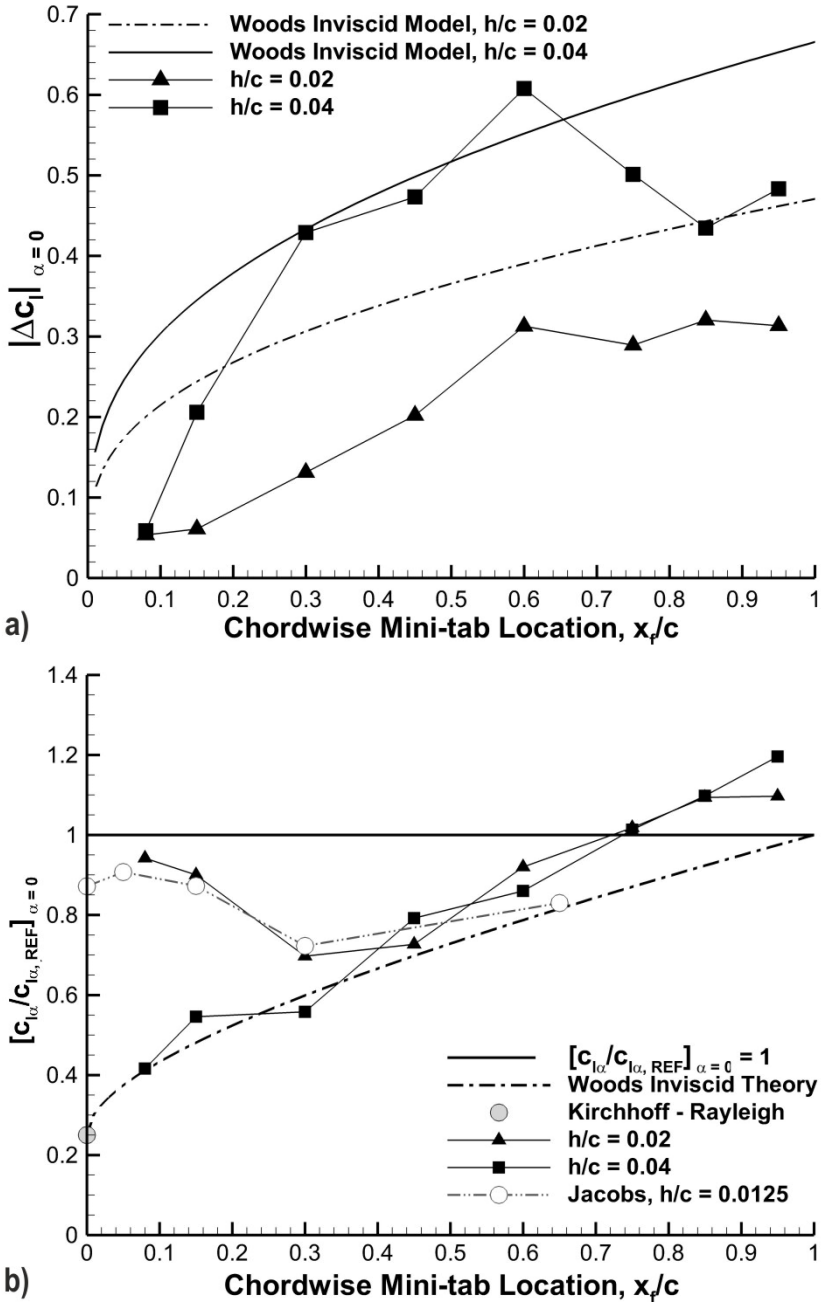

Figure 8: (a) Change in lift at $\alpha = 0°$ ($|\Delta c_l|_{\alpha = 0}$) for h/c = 0.02 and 0.04, compared to Woods [15] inviscid spoiler theory, (b) Normalised lift curve slope $[c_{l\alpha}/c_{l\alpha, REF}]_{\alpha = 0}$ vs. x_f/c for h/c = 0.02 and 0.04, compared to Woods [15] inviscid spoiler theory, Kirchhoff-Rayleigh [26, 27] theory and the experimental results of Jacobs [25] at Re = 3.1×10^6, $\alpha = 0°$.

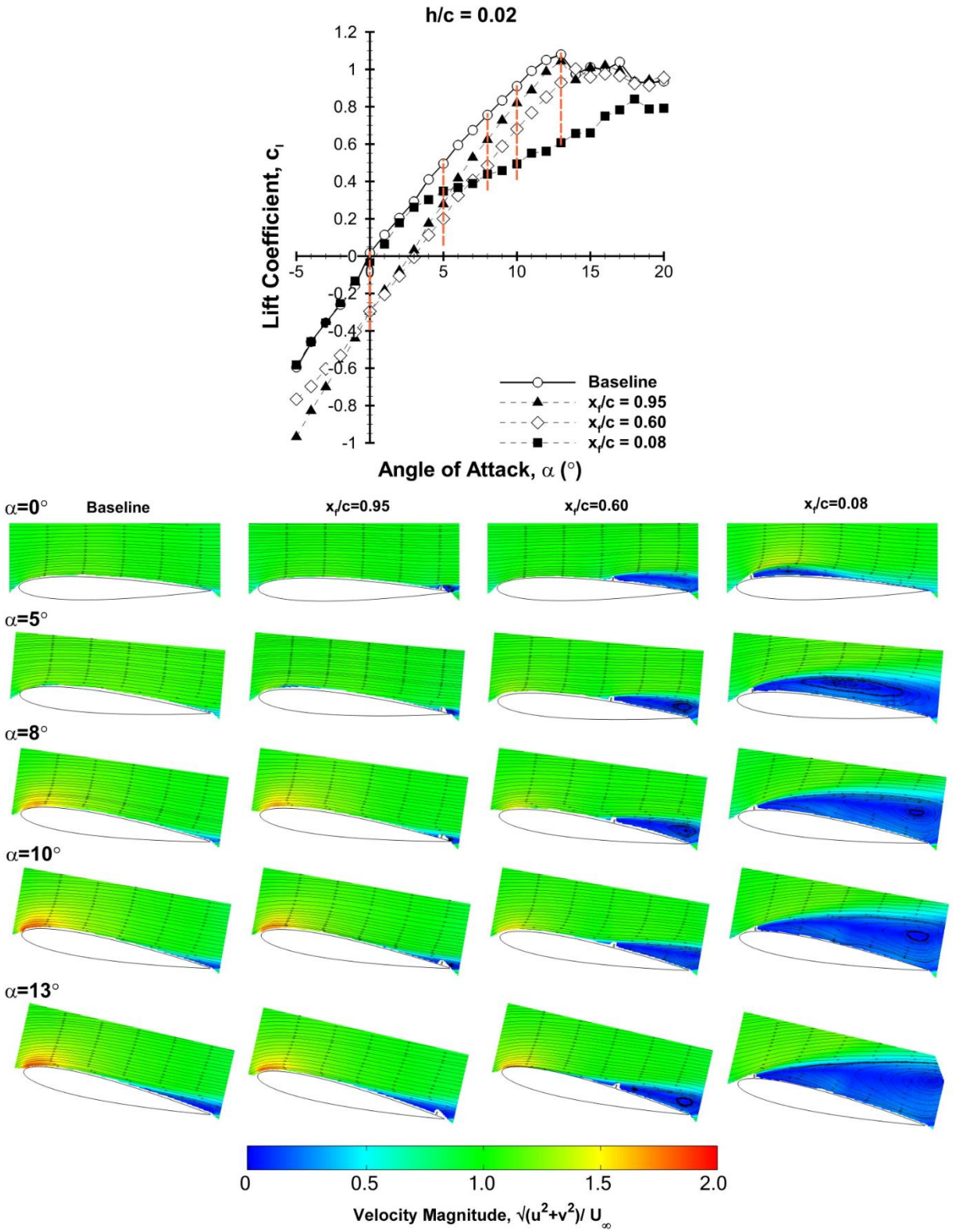

Figure 9: Lift coefficient vs. angle of attack for h/c = 0.02. Corresponding normalized velocity magnitude shown for three example chordwise locations at the angles of attack indicated by red vertical lines in the lift coefficient plot.

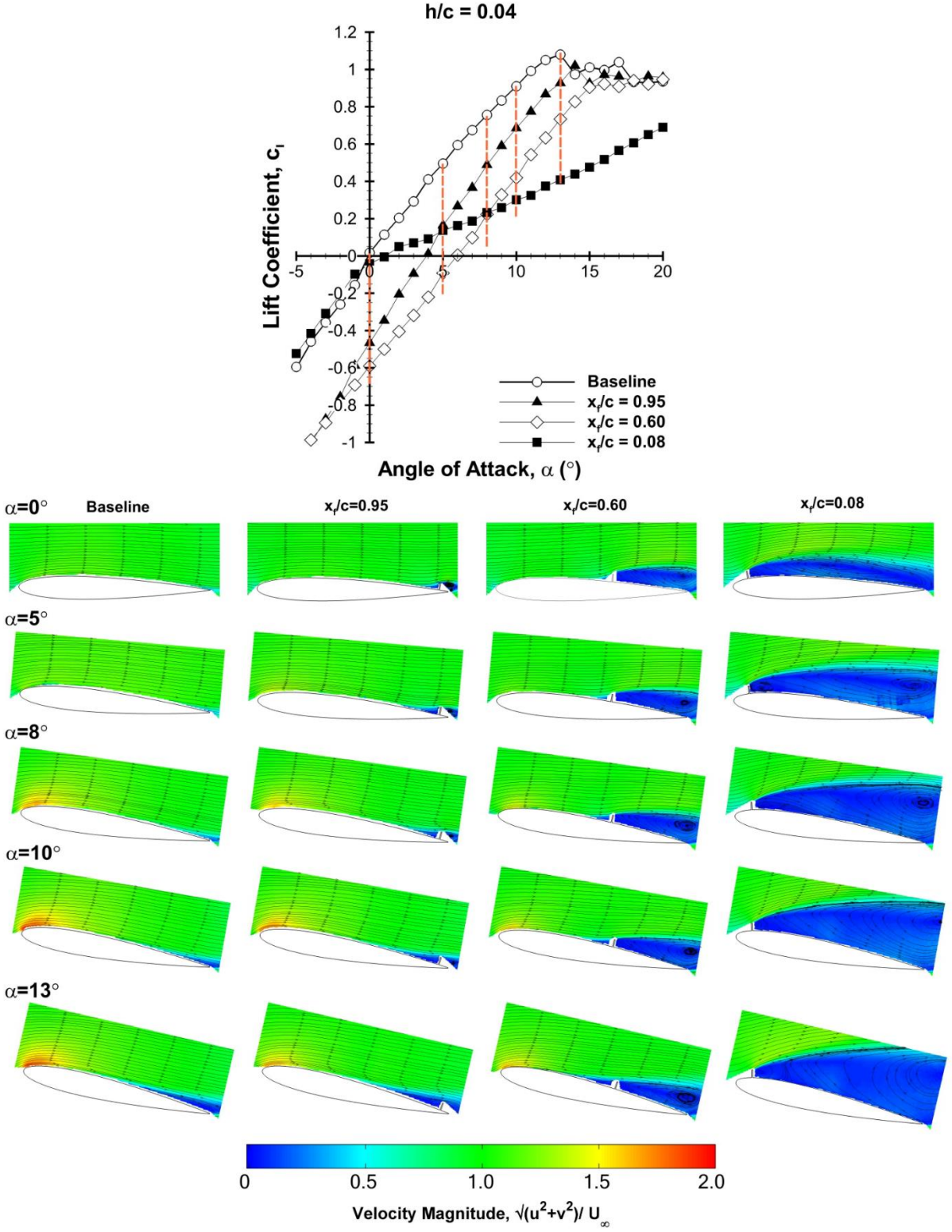

Figure 10: Lift coefficient vs. angle of attack for h/c = 0.04. Corresponding normalized velocity magnitude shown for three example chordwise locations at the angles of attack indicated by the red vertical lines in the lift coefficient plot.

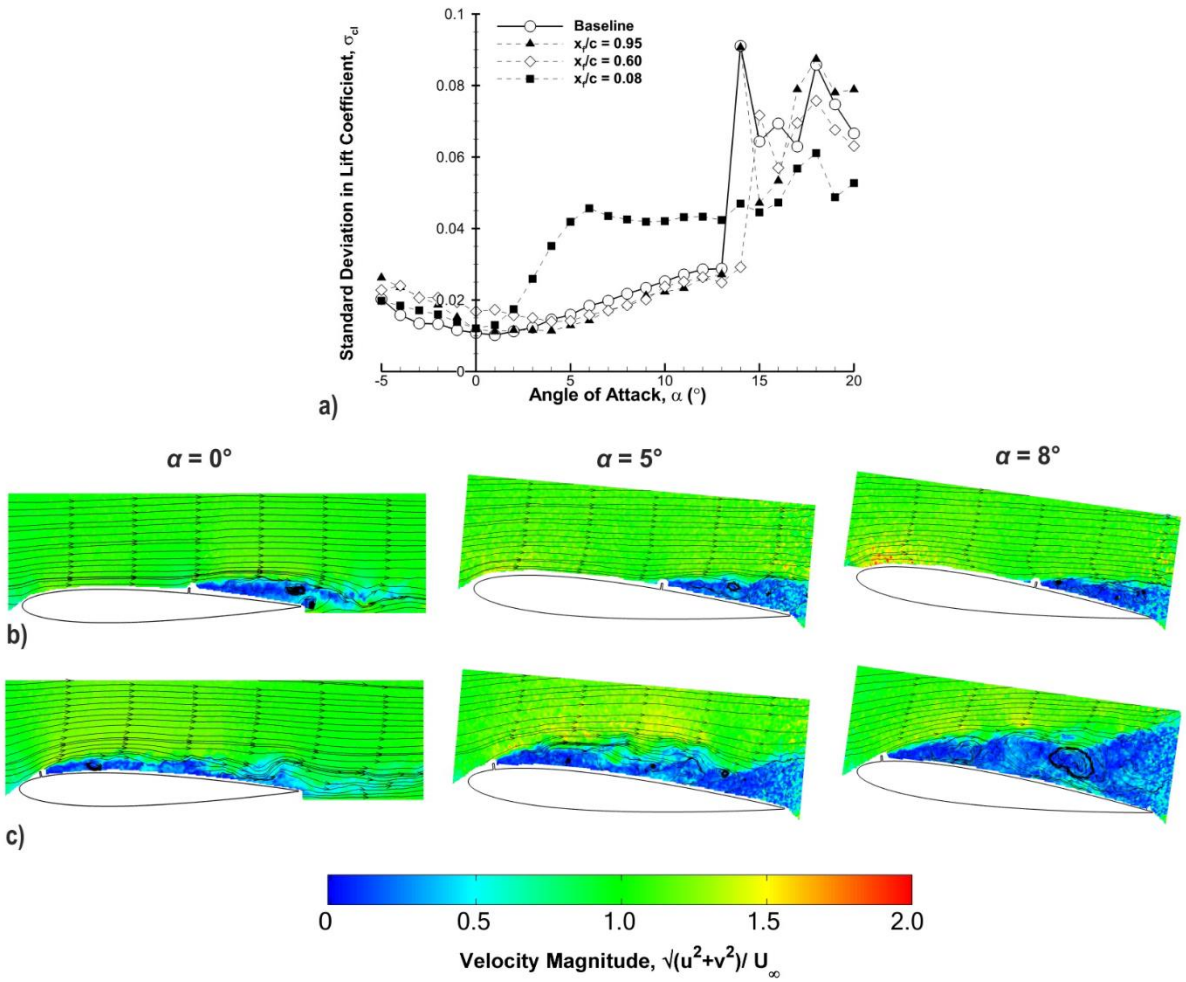

Figure 11: (a) Standard deviation in lift coefficient (σ_{cl}) for mini-tab heights of h/c = 0.02. Instantaneous normalized velocity magnitude at α = 0°, 5° and 8° presented for (b) $x_f/c = 0.60$ (c) $x_f/c = 0.08$.